CENTRIFUGE MODELLING OF DEEP EXCAVATIONS AND THEIR INTERACTION WITH ADJACENT BUILDINGS

M.Z.E.B. Elshafie (Corresponding author)

Lecturer, Laing O'Rourke Centre for Construction Engineering & Technology,

Department of Engineering, University of Cambridge,

Trumpington Street, Cambridge, CB2 1PZ, Cambridge, United Kingdom

E-mail address: me254@cam.ac.uk

Phone: 0044-1223-332780 Fax: 0044-1223-339713

C.K.C. Choy

Geotechnical Engineer, Geotechnical Consulting Group LLP

52A Cromwell Road, London, SW7 5BE, United Kingdom

E-mail address: g.choy@gcg.co.uk

R.J. Mair

Sir Kirby Laing Professor of Civil Engineering, Department of Engineering, University of Cambridge,

Trumpington Street, Cambridge, CB2 1PZ, Cambridge, United Kingdom

E-mail address: rjm50@cam.ac.uk

CENTRIFUGE MODELLING OF DEEP EXCAVATIONS AND THEIR INTERACTION WITH ADJACENT BUILDINGS

M.Z.E.B. Elshafie[1], C.K.C Choy[2] & R.J. Mair[1]

[1] University of Cambridge – United Kingdom

[2]Geotechnical Consulting Group Ltd. – United Kingdom

Abstract

Major cities in the world are experiencing a rapid growth in population while becoming increasingly overcrowded and congested. In recent years, this has created a huge demand for underground infrastructure, which often involves the design of major mass transit tunnel systems; these tunnel systems (underground tunnels and metro stations) are becoming increasingly necessary to construct in very close proximity to existing buildings. The prediction of excavation-induced deformations therefore becomes a key issue in the planning and design process for these schemes. However, current design approaches are conservative and often lead to unnecessary concern and expenditure in the design and provision of protective measures. A better understanding of the mechanisms involved in the excavation-soil-structure interaction could reduce costs and help avoid potential problems. A series of small-scale model tests was carried out in the geotechnical centrifuge at Cambridge University to investigate the interaction between excavations and model buildings. Excavations (simulated by adopting a novel two-fluid technique) in a 'free-field' were also undertaken to assess the difference between free-field ground movements and those affected by a stiff model building. A detailed description of the centrifuge models and test procedures is presented in this paper, followed by the presentation of test results that demonstrate the effect of the stiffness of the model building on the excavation induced-displacements.

Keywords: Centrifuge modelling, Excavation, Retaining wall, Deformation, Soil-structure interaction, Building Stiffness

Nomenclature

δ	Model wall friction coefficient
ϕ'	Effective angle of friction
ϕ'_{crit}	Critical state angle of friction
$\gamma_{\max}$	Maximum dry unit weight
γ_s	Shear strain in the soil
γ_{soil}	Soil unit weight
θ	Wall rotation
$\rho_{solution}$	Fluid density
ψ	Angle of dialation
d	Embedment depth (=total depth of the wall minus the excavation depth)
D_{10}	Average particle size where 10% of the mass has a smaller diameter
D_{50}	Average particle size where 50% of the mass has a smaller diameter
D_{60}	Average particle size where 60% of the mass has a smaller diameter
$e_{\max}$	Maximum voids ratio
$e_{\min}$	Minimum voids ratio
g	Earth gravity
G_s	Specific relative density
h	Excavation depth
h_{loss}	Major and minor losses in a hydraulic system
K_o	Coefficient of earth pressure at rest
K_a	Coefficient of earth pressure at active conditions
K_{int}	Coefficient of earth pressure at an intermediate stage
K_p	Coefficient of earth pressure at passive conditions
N	Number of times by which earth gravity is increased
s'	Mean effective stress
S_f	Drop in heavy fluid level
S_h	Horizontal displacements
S_w	Drop in water level
τ	Shear stress
w	Horizontal wall deflections

Introduction

Construction of excavations inevitably causes ground movements; these ground movements, particularly in highly congested urban areas, can cause adjacent existing structures to deform and possibly sustain damage[3]. Therefore, the assessment of the potential risk of damage to such structures is essential. The approach currently used to assess potential building damage for excavation (and tunnelling) projects in the UK consists of three stages (Mair et al. 1996).

In the first stage assessment, the presence of buildings is not considered; i.e. a free-field scenario is assumed. Excavation-induced 'free-field' displacements are then predicted; buildings located within a region in which small ground displacement values were predicted (lower than some pre-specified threshold) are assumed to experience negligible damage risk and are not considered further.

In the second stage assessment, buildings are modelled as elastic beams resting on the ground surface. It is then assumed that these beams will follow the free-field displacement predictions i.e. the free-field displacement predictions are imposed on the beams (Burland and Wroth, 1974; Burland et al, 1977). This approach is generally conservative (except for some buildings on individual footings) as buildings are assumed to have no effect on the free-field displacements (Burland, 1995). However, case studies from the construction of the Jubilee Line Extension (JLE) have shown that building's stiffness could affect the free-field ground displacements such that the strains sustained by the buildings are reduced (in comparison to the free-field scenario). For example, the horizontal strain measurements close to the foundations of Elizabeth House (near Waterloo Station, London) showed that the strains developing during the construction of the JLE were negligible and that those induced by thermal effects exceeded them (Standing 2001). Furthermore, Mair (2003) presented a number of case histories from the JLE (The

[3] In this paper damage relates to excavation-induced displacements only.

Treasury, Elizabeth House and Murdoch, Neptune and Clegg Houses) in which he concluded that:

- Buildings often modify free-field settlements depending on the relative building/soil stiffness.
- Horizontal strain induced in buildings is usually reduced significantly in comparison to that calculated using the free-field displacements – except possibly for some buildings on individual footings.

In summary, case studies have shown that excavation-induced ground displacements not only affect surface buildings but the stiffness of these buildings also affect the ground displacements. As a result the building's deformation are often less than the free-field scenario. Hence, the assumption that buildings have no effect on the free-field displacements is generally a conservative assumption.

In the third stage, details of the building and of the excavation (or tunnel) construction are taken into account. Building features such as the foundation design and structural continuity as well as any previous movement a building may have experienced in the past are accounted for (Burland 1995).

Much of the research undertaken to examine the effect of excavation-induced displacements on structures has mainly been based on parametric studies carried out using numerical analyses for tunnelling problems. The work of Potts and Addenbrooke (1997) and Franzius (2003) and Franzius et al. (2006) showed how the influence of soil-structure interaction can be incorporated into the second stage assessment in order to reduce the number of cases for which a detailed evaluation has to be carried out. Continuum numerical methods using finite-element computer programs offer powerful tools to model complex construction processes including deep excavations. The ability to predict excavation-induced ground movements reliably, however, is

wholly dictated by the input of representative parameters for the soil and the other structural components making the excavation. Existing numerical codes are extremely demanding of such prior information. A practical alternative to complement numerical analysis is to discover mechanisms of behaviour by means of model tests and to use them to understand the performance of buildings when subjected to excavation-induced deformations.

In order to observe these mechanisms, a research study was conducted using small-scale models tested in the 8m diameter geotechnical centrifuge at Cambridge University (Elshafie 2008). The aim of these centrifuge tests was to simulate the excavation-soil-building interaction to understand the mechanisms involved, rather than modelling a specific prototype. Therefore, it was decided to use sand for all the centrifuge tests due to the significantly smaller time required in preparation before testing compared to clay. An excavation system, which adopted a new technique for simulating the excavation process in-flight, was developed to investigate the interaction between the soil and model buildings. The test results from this research study provide new insights into the fundamental mechanisms involved. In this paper, a detailed description of the centrifuge models (and associated test procedures) is presented followed by presentation of results from two key centrifuge tests.

Description of Centrifuge Model

Strong-box and Boundary Conditions

The centrifuge model, as illustrated in Fig. 1, represents a section of a long cantilever retaining wall. The dimensions of the centrifuge model shown in Fig. 1 were determined by considering a number of factors including the capacity of the centrifuge, the magnitude of the potential soil displacements and the effects of the model boundaries on the soil movements in front of and behind the retaining wall. The model retaining wall used in this study was 225mm in height, tested at 75g, corresponding to 16.9m of a prototype wall at a scale of 1:75.

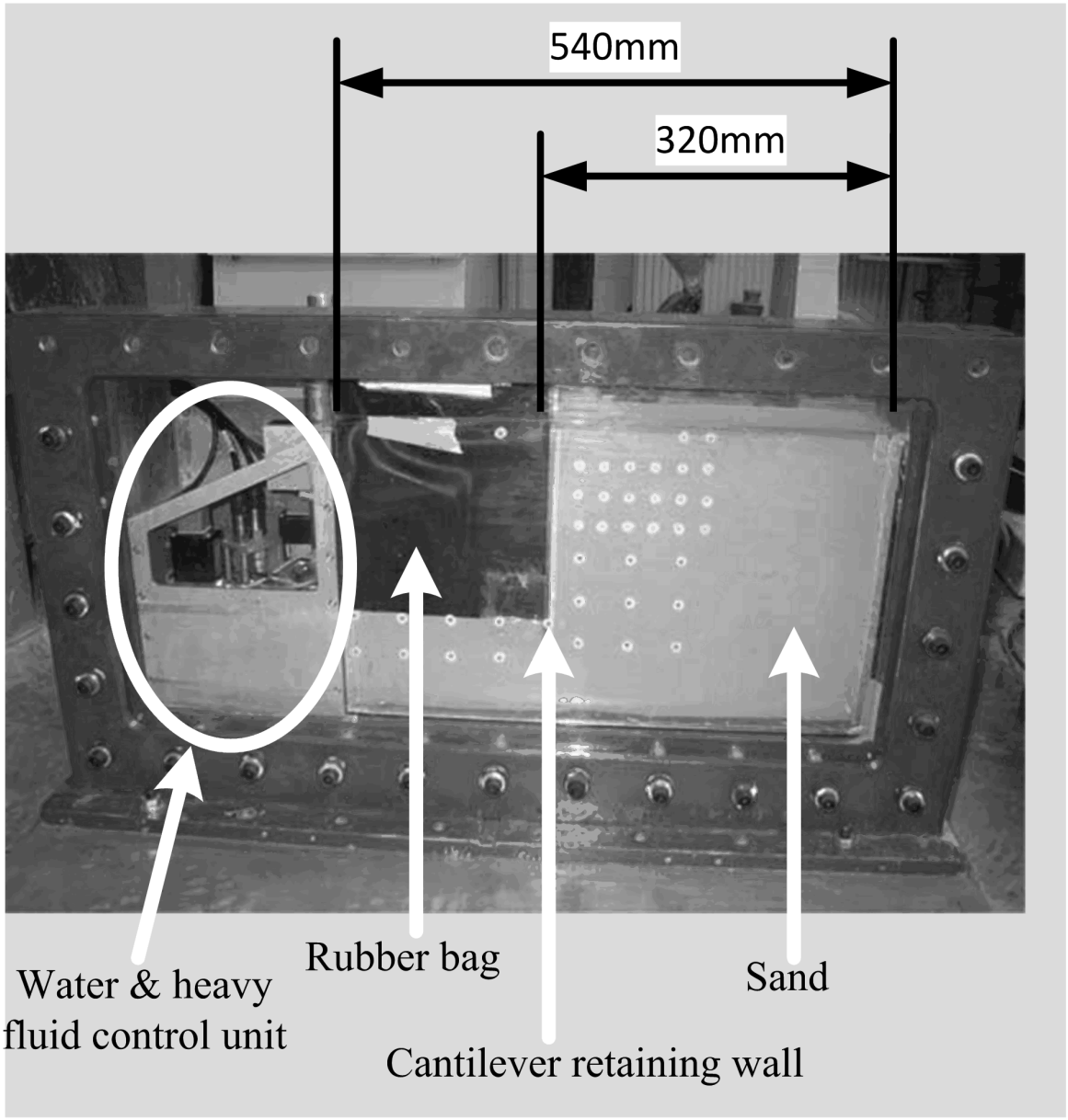

Fig. 1 – Front view of the centrifuge model

The soil movements behind the retaining wall, at working conditions, were expected to be within 1.5~2 times the excavation depth (Clough and O'Rourke, 1990); therefore the boundary of the model container was located at an adequate distance from the back of the retaining wall to ensure no boundary effects. This is illustrated diagrammatically in Fig. 2.

The centrifuge strong-box used for the model retaining wall tests had a front Perspex® window

of 80mm thickness. The Dural (an aluminium alloy) back plate was 16mm thick and had two horizontal steel stiffening beams. Conservative calculations based on formulae from Roark and Young (1975) indicated that the maximum relative lateral deflection of the window and the back plate would be of the order of 0.06mm at 75g. This implied that an out-of-plane strain of approximately 0.04% would occur as the centrifuge reached its testing speed (the width of the model box was 150 mm). This was not considered large enough to have any significant effect on the centrifuge model results.

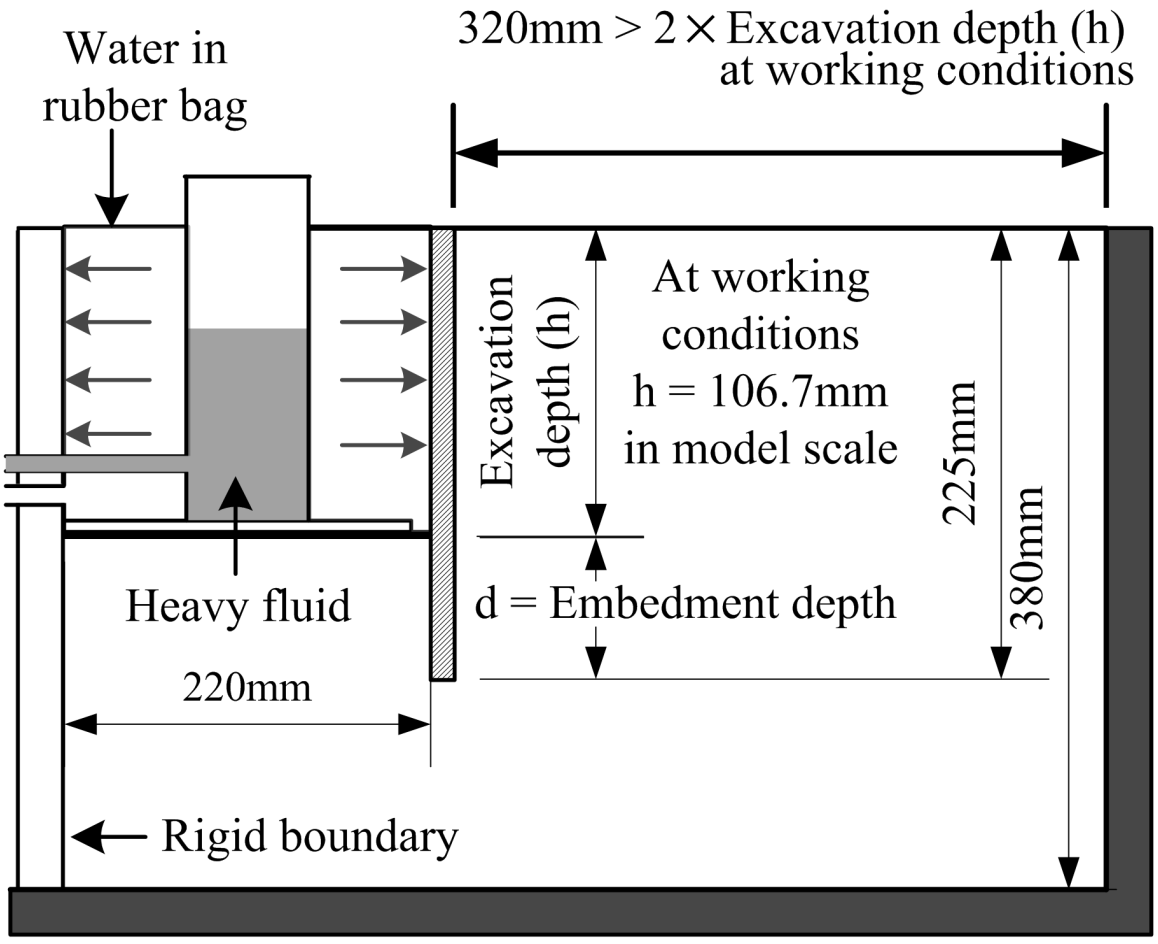

Fig. 2 Schematic diagram of the centrifuge model

Simulating the Excavation Process

Previous centrifuge modelling research on retaining wall problems have mostly relied on the use

of fluid-filled rubber bags that were drained in-flight to simulate the vertical and horizontal unloading occurring during excavation (Powrie 1986; Richards 1995; McNamara 2001). Rubber bags, which behave as a separating membrane, offer little restraint to either wall or fluid because of their low stiffness. Ideally the fluid in the rubber bag should provide a horizontal stress on the retaining wall and a vertical stress at the bottom of the excavation with the same magnitudes as those provided by the soil that should have been in its place. The sand used in all the tests in this study had an average density of about 1583 kg/m^3 ± 5%. Assuming no movement of the wall, the horizontal soil pressure exerted on the retaining wall at any depth (z) is given by:

$$K_0 \times \gamma_{soil} \times z = 7.3z \;\; kN/m^2 \tag{1}$$

where:

$K_o = 1 - \sin\phi'_{crit}$ is the coefficient of earth's pressure at rest (assuming the sand to be normally consolidated),

ϕ'_{crit} = the critical state angle of friction and

γ_{soil} is the unit weight of the sand (in kN/m^3).

Therefore, a fluid with a density of 744 kg/m^3 was required to give the same horizontal stress exerted by the soil behind the retaining wall. Silicon oils were originally considered (as they are generally lighter than water) but these fluids were either very volatile or had very low flash points which hindered their use as a supporting fluid in the centrifuge from a safety point of view. Hence it was decided to use water as the supporting fluid. Although the horizontal pressure of the water is approximately similar to that of the sand, it provided only about half the vertical stress. Therefore this difference in weight had to be compensated. Hence it was decided to use another fluid (one that was heavier than water) to balance the difference between the weight of the sand and the weight of the water; this is illustrated diagrammatically in Fig. 2. A zinc chloride solution had been widely used as a support fluid in previous centrifuge tests (e.g. Bolton and

Powrie, 1987), however, safety was a concern because of its corrosive nature; therefore a less corrosive fluid, sodium polytungstate (SOMETU Ltd.) was selected. The sodium polytungstate solution ($\rho_{solution} = 2500\ kg/m^3$) was kept inside an aluminium alloy container, which was placed inside the rubber bag. A plate was attached to the bottom of the container to distribute the weight of the fluid evenly over the entire base of excavation as shown in the diagram in Fig. 2. The plate was designed to be slightly smaller than the area at the bottom of the excavation to leave some clearance for the movement of the retaining wall. The total sum of the weights of the heavy fluid, its container, the plate attached to the bottom of the container, the rubber bag and the water inside the rubber bag should equal the weight of the sand being 'excavated'. Considering this equilibrium condition the required density and volume of the heavy fluid were determined.

It was intended to simulate the excavation in steps, each step corresponding to the excavation of the equivalent of 1m of soil in the full-scale prototype. As a result, the drainage of the water and the heavy fluid had been done simultaneously in a very controlled manner so that the right combination of removal of vertical and horizontal stresses could be achieved.

A novel approach was developed to achieve the correct combination of stresses throughout the simulation process: this approach involved designing, calibrating and adjusting the plumbing setup in three separate centrifuge tests. As the levels of the water in the rubber bag (of dimensions 220mm by 140mm in plan view) and the heavy fluid inside the aluminium alloy container (100mm by 100mm in plan view) were determined previously, the following calculations were then made:

1. In model scale, assume that the water is drained by a height of (S_w) from the rubber bag.

   The mass of the drained water is $1000 \times S_w \times [(0.22 \times 0.14) - (0.1 \times 0.1)]$ kg

2. The mass difference between the drained water and the sand should be balanced by dropping the level of the heavy fluid by an amount (S_f) in model scale
3. To ensure correct vertical stresses acting on the base of the excavation throughout the test $S_w = 0.93\,S_f$

In order to achieve the required ratio, different orifice sizes were adopted at the end of each of the water and the heavy fluid pipe systems. The drainage time that each of the two fluids would take to drain was also very important. Very high drainage speeds were not desirable, as they would not permit the excavation simulation in steps as intended. Therefore, Bernoulli's equation was used to assess the suitability of various orifice sizes for both, the water and the heavy fluid pipe systems. The calculated rate of change in height (at 75g) of the water and heavy fluid levels using different orifice sizes is shown in Fig. 3a. Based on this it was decided to use an orifice size of 2mm for the water pipe system and a 1mm orifice size for the heavy fluid pipe system. These sizes, achieved by placing aluminium alloy inserts inside a 4 mm diameter plastic pipe, should theoretically ensure that the ratio of the water to heavy fluid reduction rates was satisfied when they were drained simultaneously. They should also provide enough time for the drainage processes to control the test.

Although the pipe systems for the water and the heavy fluid were designed and assembled with great care, the required fluid reduction rates could not be achieved in the first centrifuge test (MEGF1). Two additional tests (MEGF2 & MEGF3) were carried out, in which the water pipe system was adjusted (to increase or decrease the head loss), in order to calibrate the in-flight control system. The fluid reduction rates obtained from test MEGF3 are shown in Fig. 3b. The ratio of the rate of reduction in the level of water to the rate of reduction in the level of the heavy fluid is 0.96. This compared well with the theoretical value of 0.93 required to ensure correct vertical stresses on the base of the excavation. The setup controlling the drainage of the

fluids from the rubber bag and the heavy fluid container is shown in Fig. 4. The heavy fluid was collected inside the catch tank shown while the water was allowed to pour out of the package and onto the floor of the centrifuge facility.

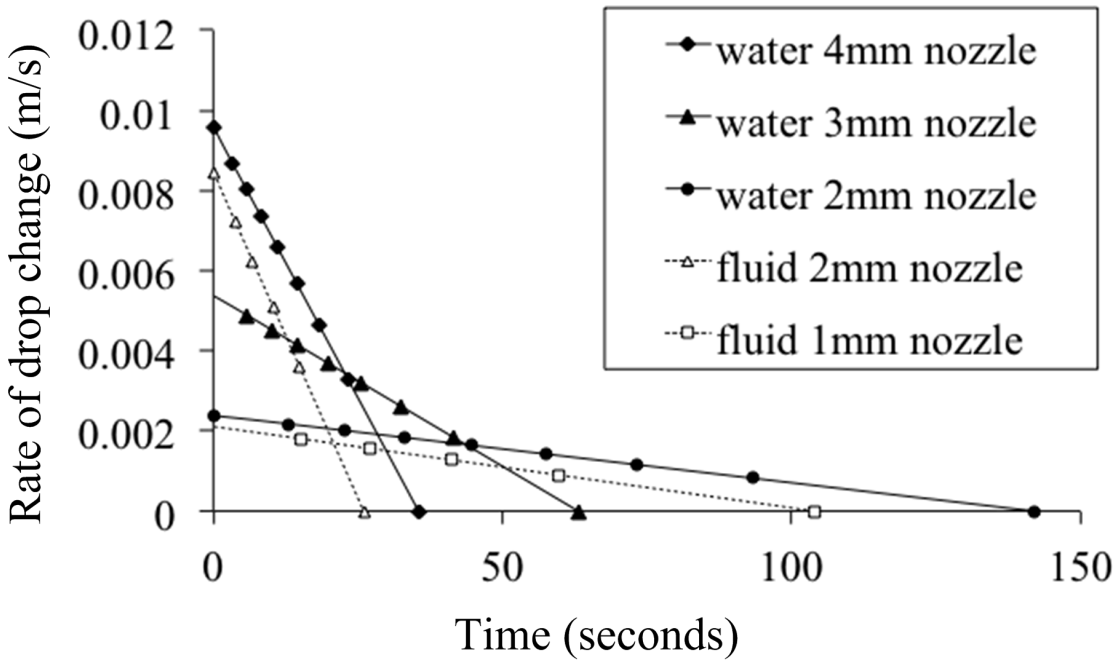

(a)

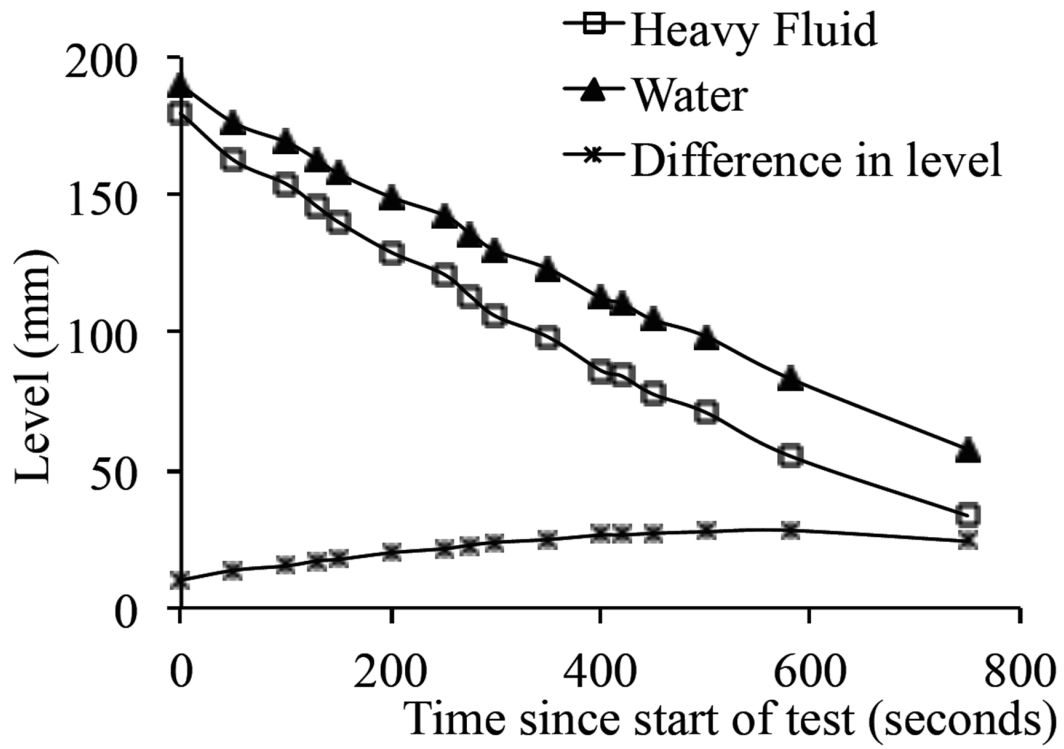

(b)

Fig. 3 (a) – Rate of drop change for water and heavy fluid
(b) – Water and heavy fluid levels measured at 75g

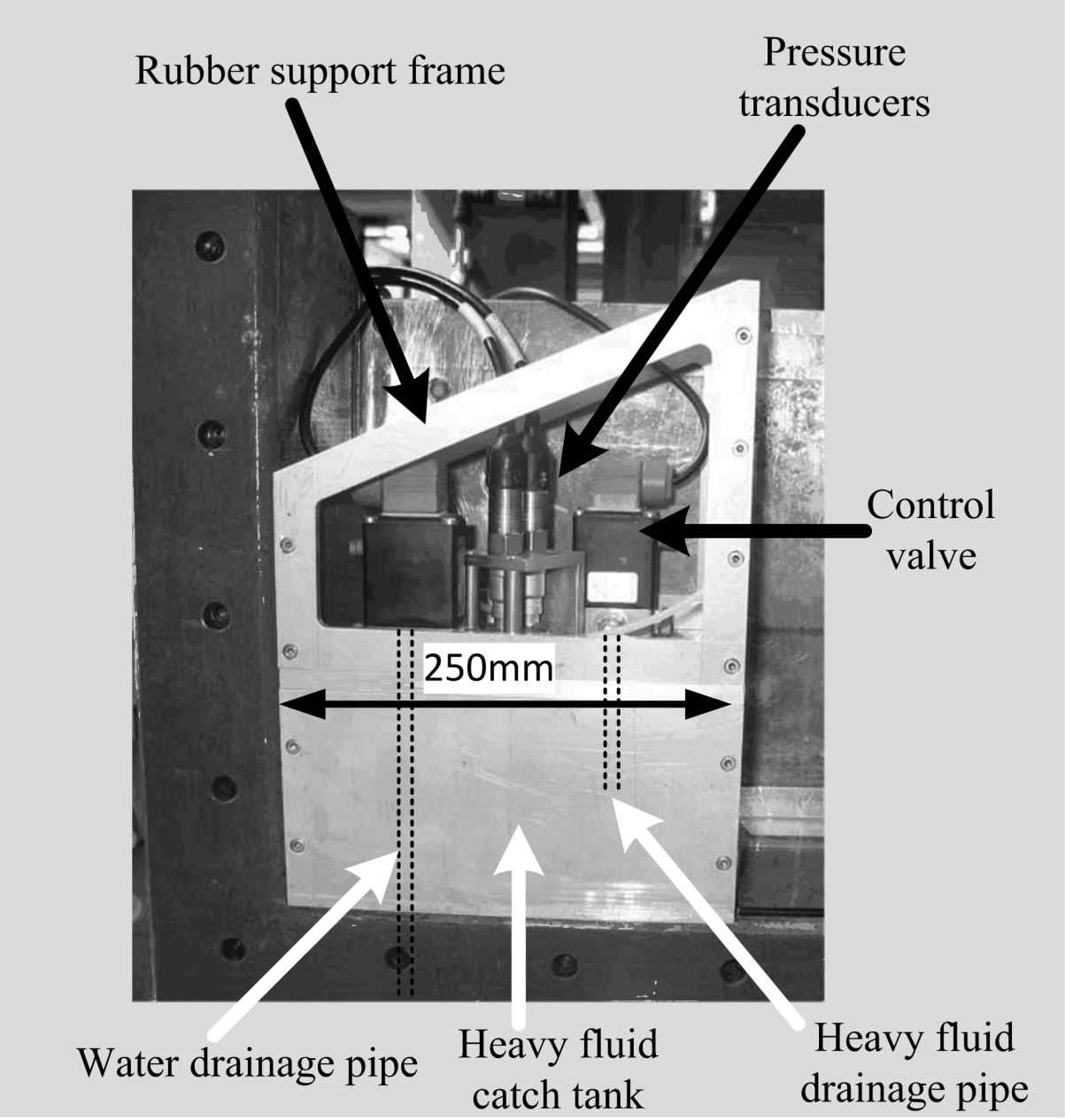

Fig. 4 – Water and heavy fluid drainage control setup

Model Wall

The model wall used during the centrifuge tests was 225 mm in length and 138mm in width. It was machined with an additional rectangular piece at the top which served as a target for a laser sensor used to measure the horizontal wall displacements (w). The model wall was machined from aluminium alloy sheet (Grade HE30TF, conforming to BS 1474) with a thickness of 4.76mm. The centrifuge strong-box provided a space of 540 mm (length), 360 mm (height) and

150 mm (width) for the soil sample. In order to minimise friction between the sand and the strong-box boundaries, it was decided to use two pieces of glass between the box boundaries and the soil. This followed from the work done earlier at Cambridge by Arthur (1962) in which he showed that the shear strains in a plane close to the glass sides and a plane far away from the sides were very similar, indicating that the glass was effective in minimising friction. This method was found to be effective in reducing the friction in this research, as will be presented later. The glass was laminated in order to prevent it from breaking into fragments in case a crack opened. The total thickness of the glass on the boundary of the strong-box was 10mm leaving the soil occupying a width of 140 mm.

The width of the wall was set to be 138 mm so that a gap of 1 mm was left on either side of the wall when placed at the centre. These gaps ensured no contact between the wall and the sides of the box; however, this allowed sand to flow through the gaps to the other sides of the wall. This was prevented by using paper and plastic film ('Cling film') along the entire height of the wall as shown in Figs. 5a & 5b. In Fig. 5a the plastic film is shown stretched which is the condition encountered after the commencement of the excavation process. Prior to the test the plastic film was folded; one end of the paper was fixed to the glass and the other was fixed to the plastic film, which had the other end fixed to the model wall. This way the wall was not restrained from moving during the test and sand was prevented from occupying the space between the model wall and the glass.

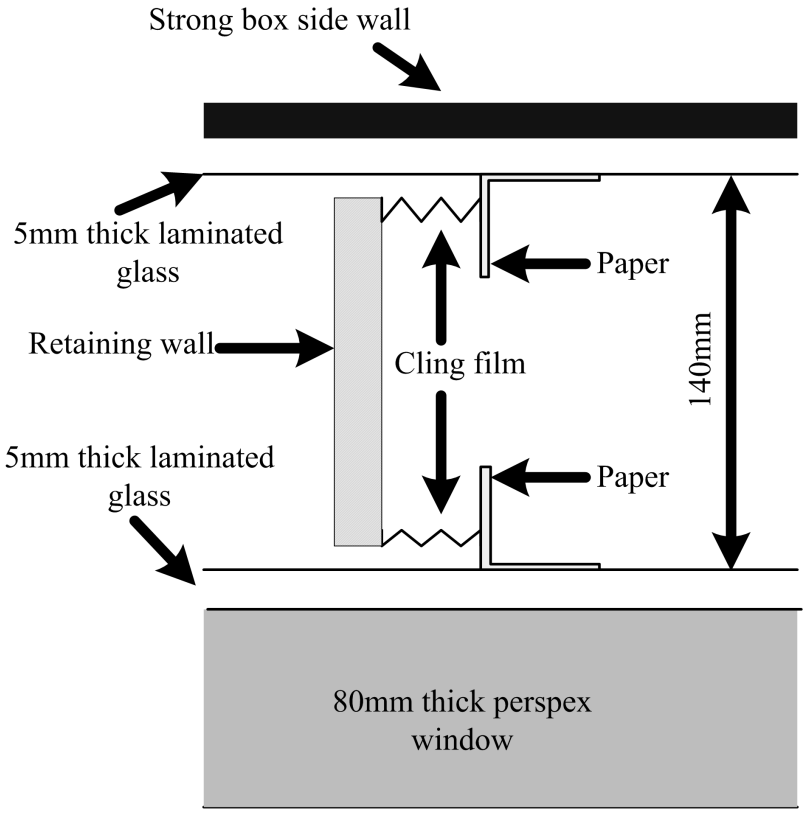

(a)

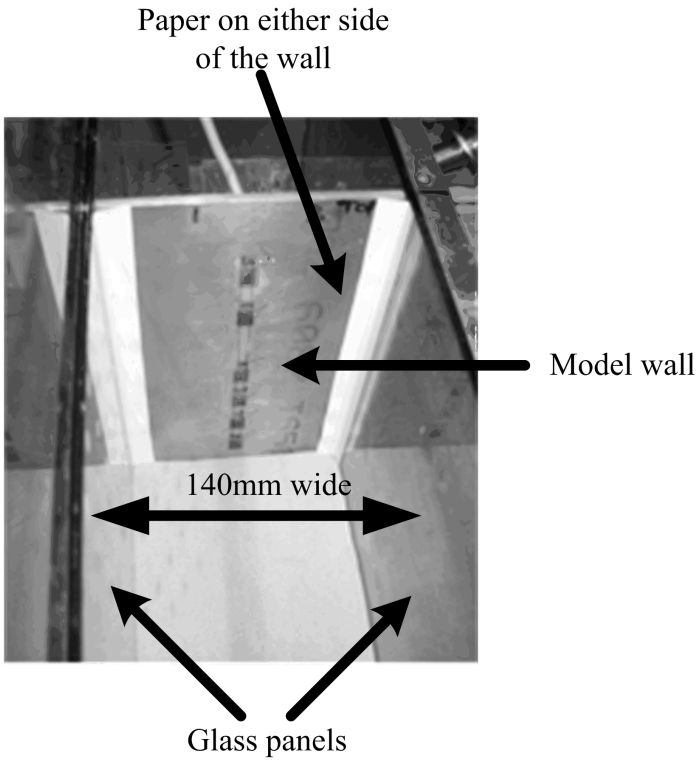

(b)

Fig. 5 (a) – Schematic plan view of the model wall and strong box arrangement (**b**) – Picture of the model wall located inside the strong box during preparation

Model Preparation

Sand Properties and Sand Pouring

Dry silica sand, Fraction E – Grade 100/170 – size (0.09- 0.015mm) was used in the centrifuge tests. The D_{10}, D_{50} and D_{60} grain sizes were 0.095, 0.14 and 0.15mm, respectively. It had a minimum voids ratio, $e_{\min}$ of 0.65 ($\gamma_{\max} = 16\ kN/m^3$) and a maximum voids ratio, $e_{\max}$ of 1.01 ($\gamma_{\max} = 13.3\ kN/m^3$). The specific gravity G_s was 2.67 and the critical state angle, $\phi'_{crit} = 32^o$ (Tan, 1990). The sand used in all the tests in this study had an average density of about 1583 kg/m^3 (relative density = 90%) ± 5%. A robotic sand-pouring machine (Madabhushi et al., 2006) was used to prepare the soil samples for all the centrifuge tests reported in this paper. The machine adopts the multiple sieve dry pluviation method using an automatically controlled nozzle that can travel along any 3-dimensional path in space at a range of speeds. Using this setup, Zhao et al. (2006) demonstrated that the variation of the sand density obtained in the soil samples was typically in a range of ± 5 % of the mean value.

Model Instrumentation

The instrumentation adopted in a typical centrifuge test is shown in Figs. 6a and 6b. The deformations of the sand and the wall were measured by an integrated system of instruments with an adequate degree of redundancy. This provided a useful feedback not only on the reliability of the system but also on any deficiencies or unusual aspects that might have existed in the model.

A combination of four linear variable differential transformers (LVDTs) supplied by Solartron and five laser displacement sensors with 16-26mm measuring range (OADM 12I6430/S35A) supplied by Baumer Electric, were used to monitor the soil settlement behind the wall and the

horizontal movement of the wall. The laser sensors and LVDTs were all installed on a plate, which was resting on the gantry. This is shown in more detail in Fig. 6c – the figure also shows the location of the laser sensors and the LVDTs relative to the retaining wall. Laser1 and LVDT1 were arranged to record the movements of the soil at the same distance behind the wall, checking the consistency of the instruments. The remaining laser sensors were arranged to measure the soil displacement profiles independently. The soil settlement profiles based on the laser sensors and LVDTs could be compared to check the compatibility of the readings.

A separate laser sensor with a range of 100-500mm (OADM 2014471/S14C, Baumer Electric) was allocated to trace an aluminium target that is fixed at the top of a thin hollow tube with a buoy attached to it at the bottom end. The target, tube and the buoy were all placed inside a 25.4mm (1-inch) diameter copper tube, which was connected through a pipe to the rubber bag containing the water. During the centrifuge test, the water level in front of the retaining wall dropped, and consequently the level of the water inside the copper tube also dropped at the same time. The buoy would move down by the same amount, which was recorded by the laser sensor aimed at the aluminium target. Therefore the level of the water in front of the retaining wall could be obtained accurately. The aluminium target, the laser, the copper tube and the buoy are shown in Figs. 6a and 6b. A polytetrafluoroethylene (PTFE) cap served as a guide for the thin hollow tube to prevent it from flexing at high g-levels.

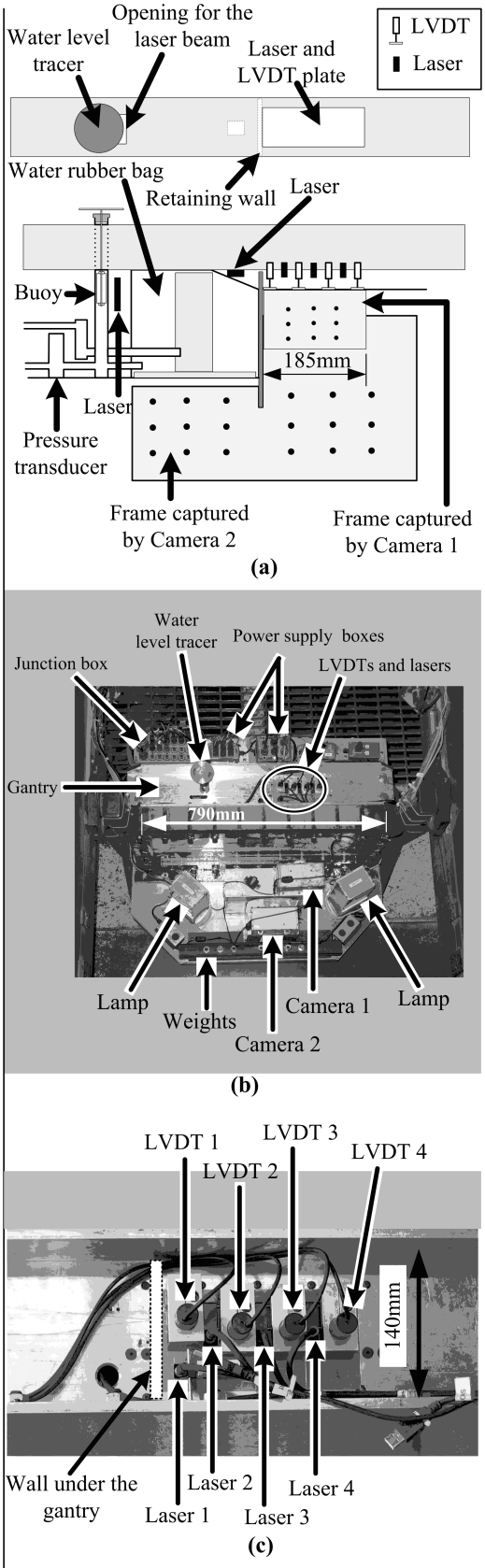

Fig. 6 (a) – Schematic view of the instrumentation in a typical centrifuge model **(b)** – Picture of a centrifuge model loaded into the beam – some instrumentation indicated **(c)** – Arrangement of the LVDTs and lasers in relation to the retaining wall

In one of the later tests, a micro-concrete block (simulating a building) would be placed on top of the soil surface behind the retaining wall and therefore the laser sensors and LVDTs would not be able to measure the soil displacements beneath the block. Therefore it was decided to use PIV - a deformation measurement system based on particle image velocimetry and close-range photogrammetry, as detailed by White et al. (2003). It makes use of digital photography to capture images of planar soil deformations. The movement of a fine mesh of soil patches (a patch consists of a known number of pixels) is measured with high precision and traced in any desired number of images. The setup for the PIV used in the tests is shown in Fig. 7. The two cameras shown in the figure were located to capture the frames shown in Fig. 6a during testing.

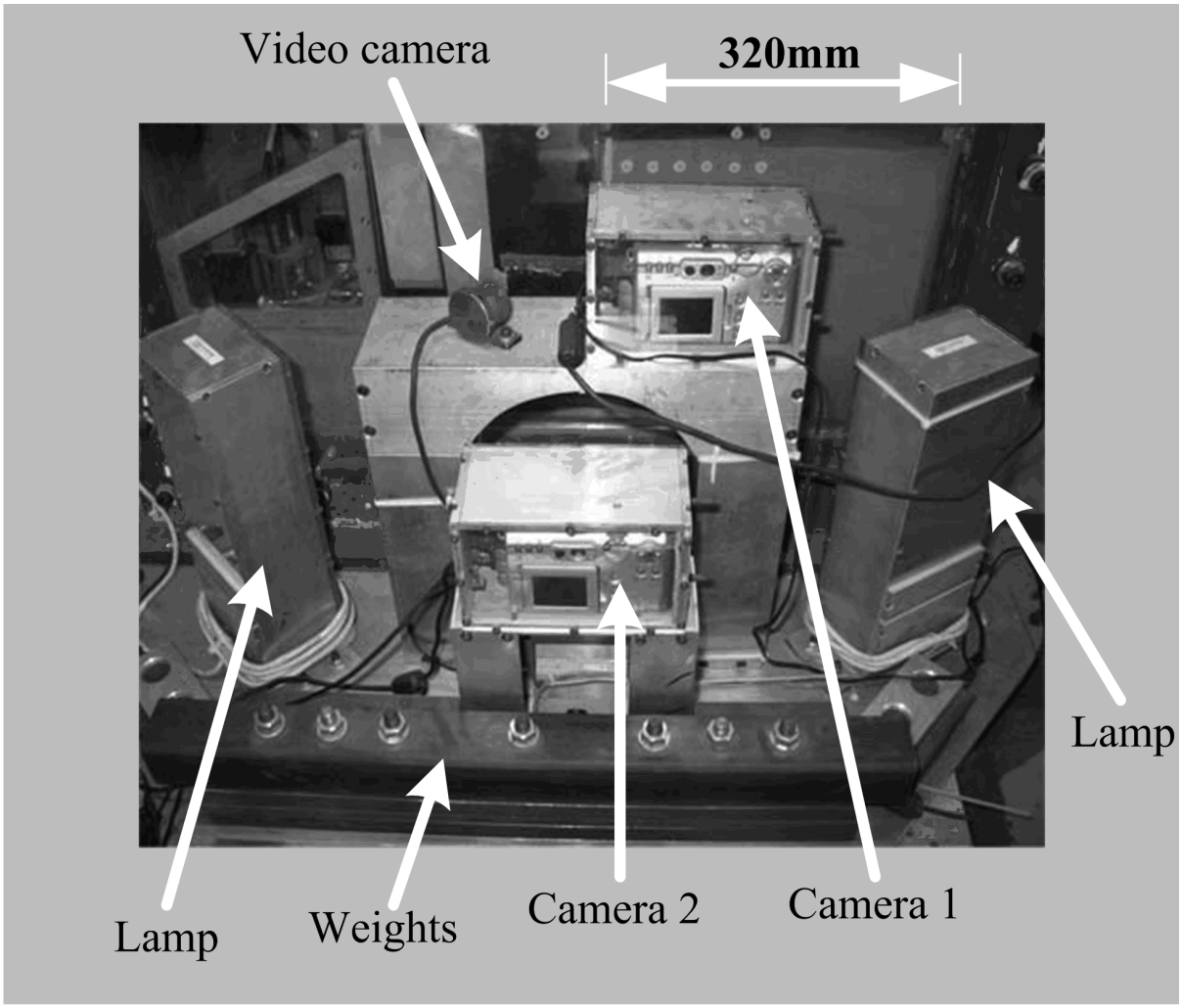

Fig. 7 – PIV arrangement used in the models

Testing Procedure

A standard testing procedure was followed for all centrifuge tests reported in this paper:

1. The package was loaded on to the centrifuge and the beam was accelerated in increments of 10g up to 60g after which the 75g level was reached in one increment
2. At 75g, an automatic control of the solenoid valves was switched on. It was adjusted to open the two valves (for the water and for the heavy fluid) simultaneously for six seconds, which resulted in approximately a 1m-excavation depth in prototype scale. The pressure transducers (for the water and heavy fluid) were closely monitored throughout the test to check for any leakage.
3. The automatic valve controller was set to have a 30-second gap between every excavation increment for taking digital pictures.
4. Excavation proceeded until the wall collapsed, after which the test was stopped.

Two test results are reported in this paper; MEGF3 represents the free-field scenario while test MEST3 represents the case when a stiff micro-concrete block, simulating a building, is located at very close proximity to the edge of the model excavation. The soil and model building deformations are compared and the mechanisms of behaviour are discussed.

Summary of Test Results

Modelling Limitations

As detailed earlier, the simulation of the excavation process was performed by the drainage of water and a heavy fluid simultaneously in front of the retaining wall. The wall would remain 'at rest' and not displace if the earth pressure (at rest) on the retained side exactly balanced the water pressure from the rubber bag on the other side. In practice this was not possible, and hence, the wall was expected to move inwards towards the retained soil (as the water pressure is slightly larger than the earth pressure 'at rest') during the acceleration stage from 1g to 75g at which the

tests were performed. The soil and wall displacements were recorded during the acceleration stage at 10g, 20g, 40g, 60g and 75g. Fig. 8a shows the horizontal movement of the top of the retaining wall (towards the retained soil) with increasing g-level. At 75g the top of the wall had moved 0.7mm at model scale towards the retained soil.

Fig. 8b shows the development of soil settlement behind the wall, with increasing g-level (at 1g the sand surface was level). The surface soil settlement curves were the result of three factors: soil settlement due to the increase of the g-level, the effect of friction between the wall and the adjacent soil and the effect of wall displacement towards the retained soil, as discussed above. The soil region adjacent to the retaining wall was affected by the roughness of the wall surface with this effect decreasing away from the wall. Fig. 8c shows the cumulative soil horizontal displacements at 75g. The negative values of soil horizontal displacements indicate that the soil behind the wall moved away from the excavation (towards the retained soil) with the displacements decreasing away from the edge of the excavation. The horizontal displacements level out to a movement of about 0.3mm away from the wall implying uniform horizontal compression; the larger horizontal soil displacements measured adjacent to the wall, are due to the horizontal displacement of the wall.

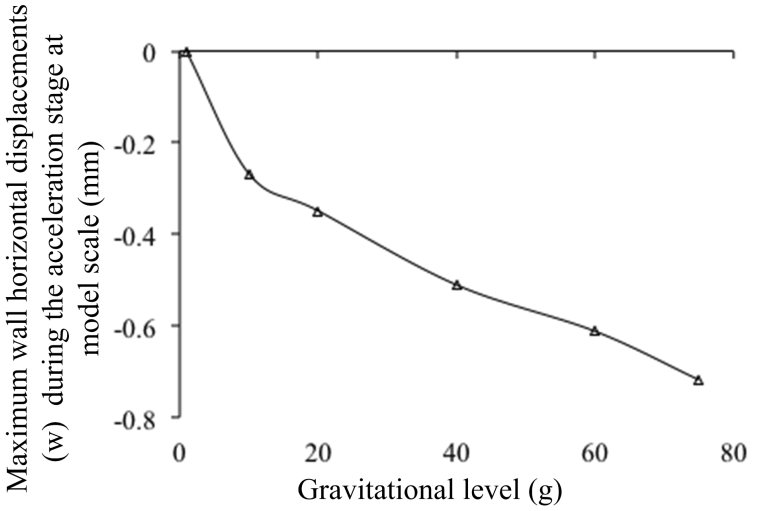

(a)

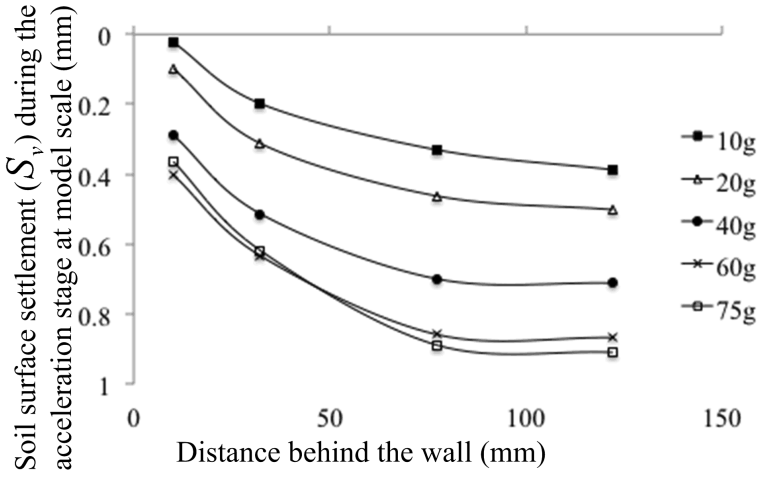

(b)

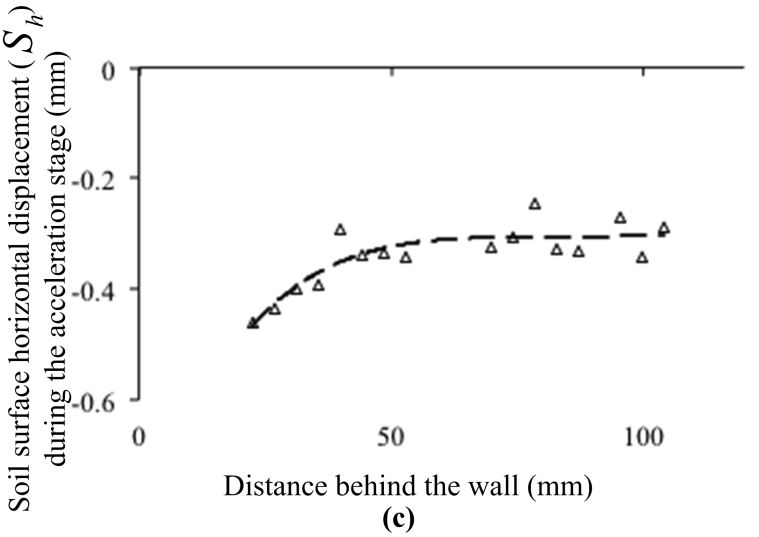

(c)

Fig. 8 (a) – Retaining wall horizontal movements with increasing gravitational force **(b)** – Soil settlement behind the wall with increasing gravitational force (as measured by the lasers) **(c)** – Soil horizontal displacement behind the wall at 75g (measured using PIV)

Terzaghi (1934a, 1934b) in his experiments on hinged walls in sands has shown that the strains required to mobilise the active earth pressure are much smaller than the strains required to mobilise the passive earth pressure. Clayton and Milititsky (1986) re-plotted Terzaghi's experimental data as shown in Fig. 9a. The active earth pressure is fully mobilized at an average shear strain of about 0.2% ($S_h / h = 0.001$), whereas the passive earth pressures are fully mobilised at an average shear strain of about 4% ($w/h = -0.02$). For the purposes of this study the ratio of lateral wall displacement to the height of the retaining wall is a measure of average shear strain in the soil. Bransby and Milligan (1975) relate the wall rotation, θ, dilatancy angle ψ, and the shear strain γ_s as follows:

$$\gamma_s = 2 \times \sec\psi \times \theta \tag{2}$$

For small angles of rotation:

$$\theta \cong \tan\theta = w / h \tag{3}$$

The above assumption was considered reasonable for small angles of dilatancy. Assuming that the retaining wall of test MEGF3 had rotated about its toe,

$$w / h = -0.7 / 225 = -0.0031 \tag{4}$$

with an average shear strain of 0.62%. Substituting the value of S_h / h in Fig. 9a gives a value of $K_{\text{int}} = 1.3$ for the coefficient of earth pressure (the subscript means that at this stage the earth pressure coefficient is at an intermediate stage between the 'at rest' K_o value and the passive earth pressure coefficient K_p). Ideally the wall should not move (the earth pressure behind the retaining wall would be at a K_o condition) in which case the soil displacements would be zero. The effect of the inwards wall displacement on soil displacements is difficult to estimate. For a soil element A (see Fig. 9b) behind an imaginary retaining wall that remained stationary during the acceleration stage of the centrifuge test, the stress path (during the excavation stage) in plane strain (with axes of shear stress, τ, and mean effective stress, s') starts at point 1 and reaches

the K_a line at point 2 in the figure; this assumes the wall moves outwards sufficiently to fully mobilize the active state. For a soil element B behind a retaining wall that had moved towards the retained soil, the stress path ends up at a point 3 after the acceleration stage has finished, and then reverses in direction during the excavation stage as it goes from point 3 and finally reaches the K_a line at point 4. Although the stress path between points 3 and 4 is longer than the stress path between points 1 and 2 for element A, it is not possible to conclude that more displacements are expected for element B. This is because the stress path of element B experiences a reversal, which makes its response along the path 3-4 stiffer at the beginning with the stiffness decreasing along the stress path. Therefore comparison of displacements for elements A and B is difficult to estimate. As the objective of the free-field test was to determine the wall and soil displacements due to the simulated excavation, the soil settlement and horizontal profiles that had occurred when 75g was reached were taken as the reference displacement profiles; all displacements reported in this paper are relative to these reference profiles.

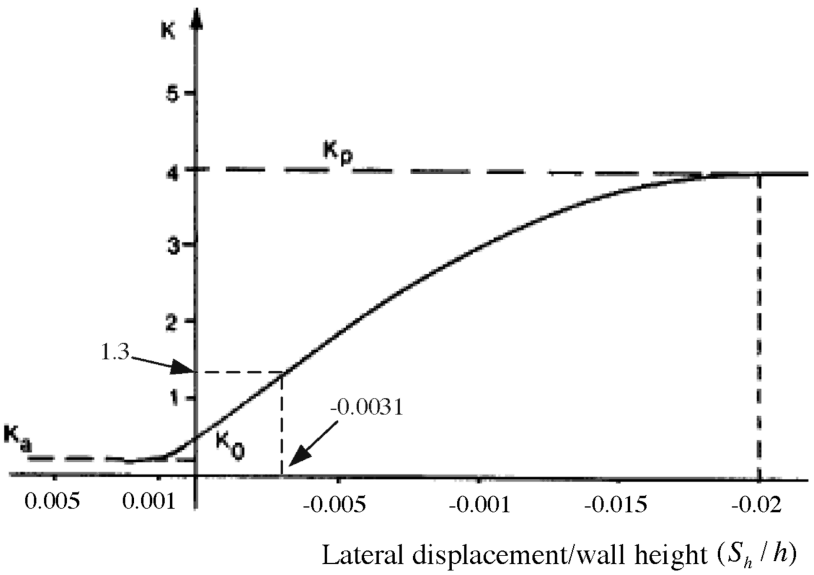

(a)

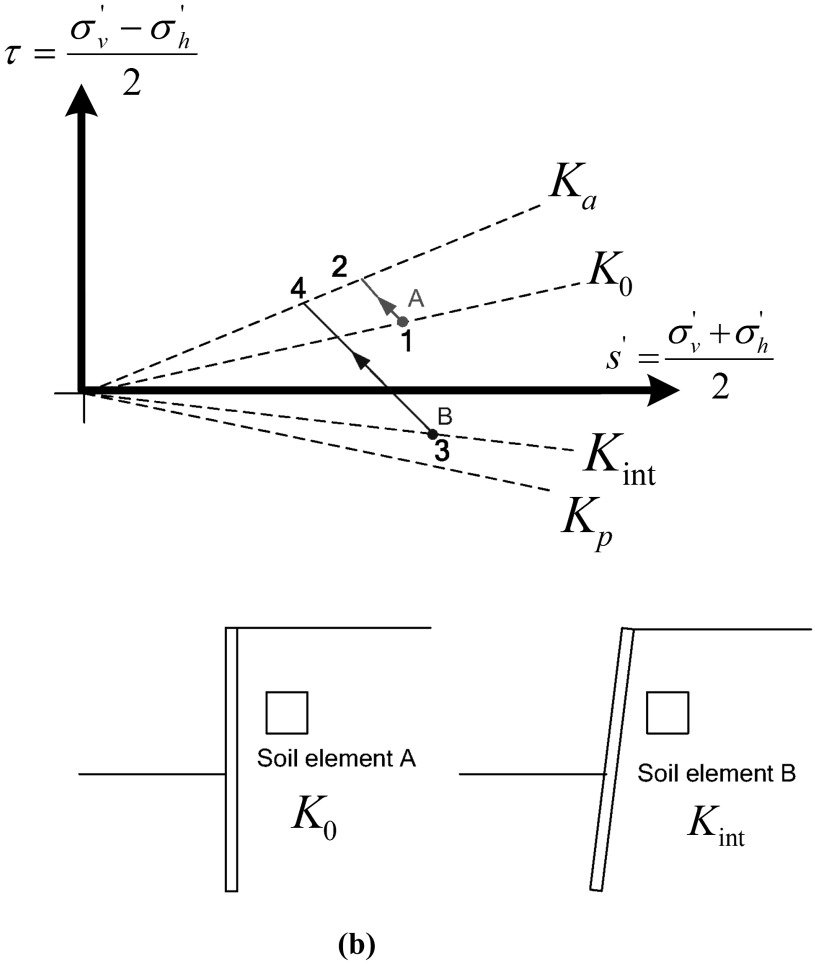

(b)

Fig. 9 (a) – Strains required for mobilisation of active and passive earth pressures (after Clayton and Milititsky. 1986) **(b)** – Stress paths comparison for soil elements A and B with different initial stress conditions

Free-field Tests

The surface soil settlement measurements from the LVDTs and the lasers were plotted for different excavation levels in Fig. 10a according to the relative location of the instruments behind the wall. All the measurements shown in Fig. 10a are laser transducer measurements except those marked as LVDT measurements. The lines shown are the best-fit lines through all the measurements, lasers and LVDTs. The settlement measured by the lasers and LVDTs were consistent, showing similar soil settlement profiles at different excavation levels. The displacements at an excavation depth of 106.7mm (8m excavation in prototype) represent the soil settlement at working conditions, i.e. at a factor of safety for strength against overturning of about 1.5. In normalised form the corresponding maximum soil settlement recorded was 0.28%h (where h is the excavation depth). The factors of safety were calculated following the simplified pressure distribution at limiting conditions (Padfield and Mair, 1984). Fig. 10b shows the soil surface settlement profile at model scale at different excavation depths as observed by the field of view of camera 1. The profiles show the magnitude and curvature increasing with increase of the depth of excavation, as expected for a cantilever wall. The settlement profiles obtained from the PIV are for the soil in contact with the glass sheet. Comparison with the readings of the lasers and LVDTs in Fig. 10a gives a measure of how efficient the laminated glass sheets were in reducing friction.

Fig. 10c shows the soil surface horizontal displacements profile behind the wall at model scale with increasing depth of excavation. The horizontal displacements were large close to the retaining wall and decreased away from the wall. Compared to the soil settlements, also recorded by PIV, the horizontal displacements were of very similar magnitude. Fig. 10d shows the maximum horizontal wall displacements normalised by the excavation depth (h). The corresponding prototype excavation depths are also indicted in the figure. At working conditions (prototype excavation depth of 8m) the normalised maximum horizontal wall displacement was about 0.4%h.

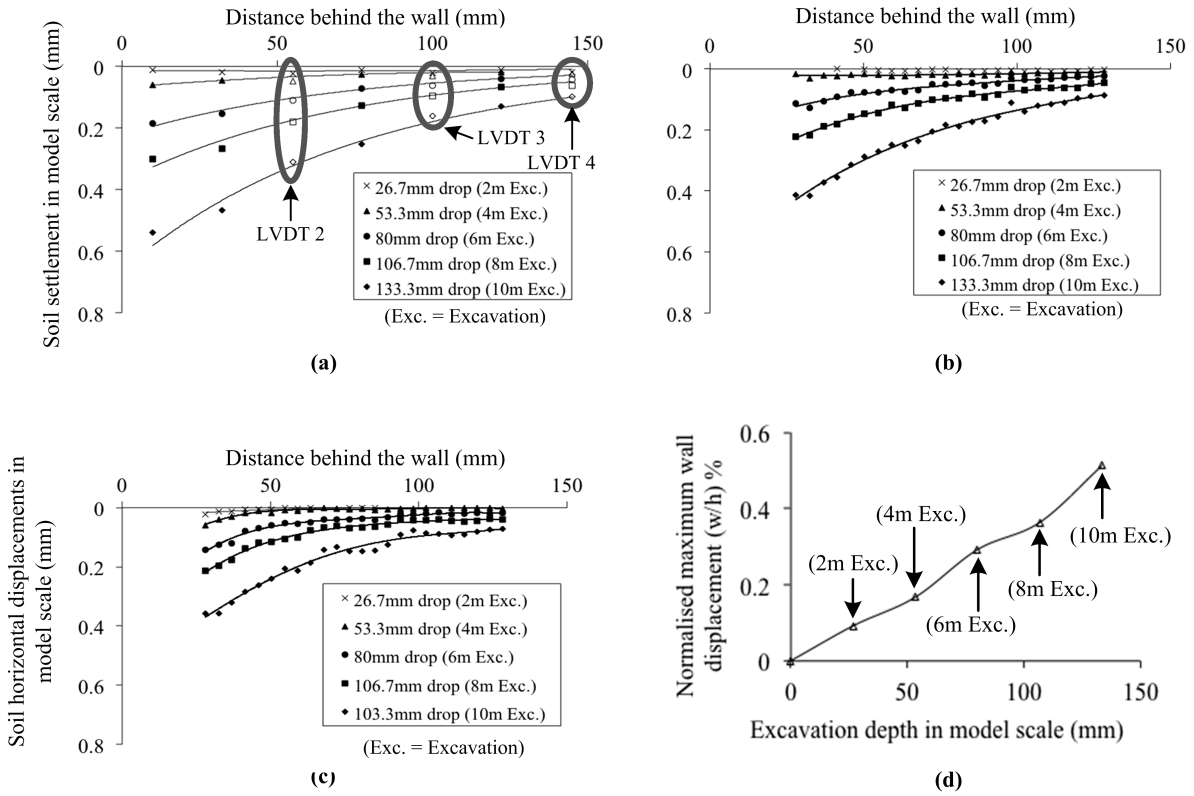

Fig. 10 (a) – Surface soil settlement (in model scale) behind the wall with increasing depth of excavation – laser and LVDT measurements **(b) –** Surface soil settlement (in model scale) behind the wall as measured by PIV **(c) –** Surface soil horizontal displacement (in model scale) behind the wall as measured by PIV **(d) –** Normalised maximum horizontal wall displacements with increasing depth of excavation

The layout of the lasers and LVDTs was designed such that each instrument could be checked by the two adjacent ones. For example each laser was placed between two LVDTs, which provided upper and lower limits for the laser reading. Laser 1 and LVDT1 were both located 10mm behind the retaining wall to check the assumption of plane strain. Fig. 11 shows the displacements (at model scale) recorded by Laser 1 and LVDT 1 during the test. The two instruments agreed very well, validating the plane strain assumption.

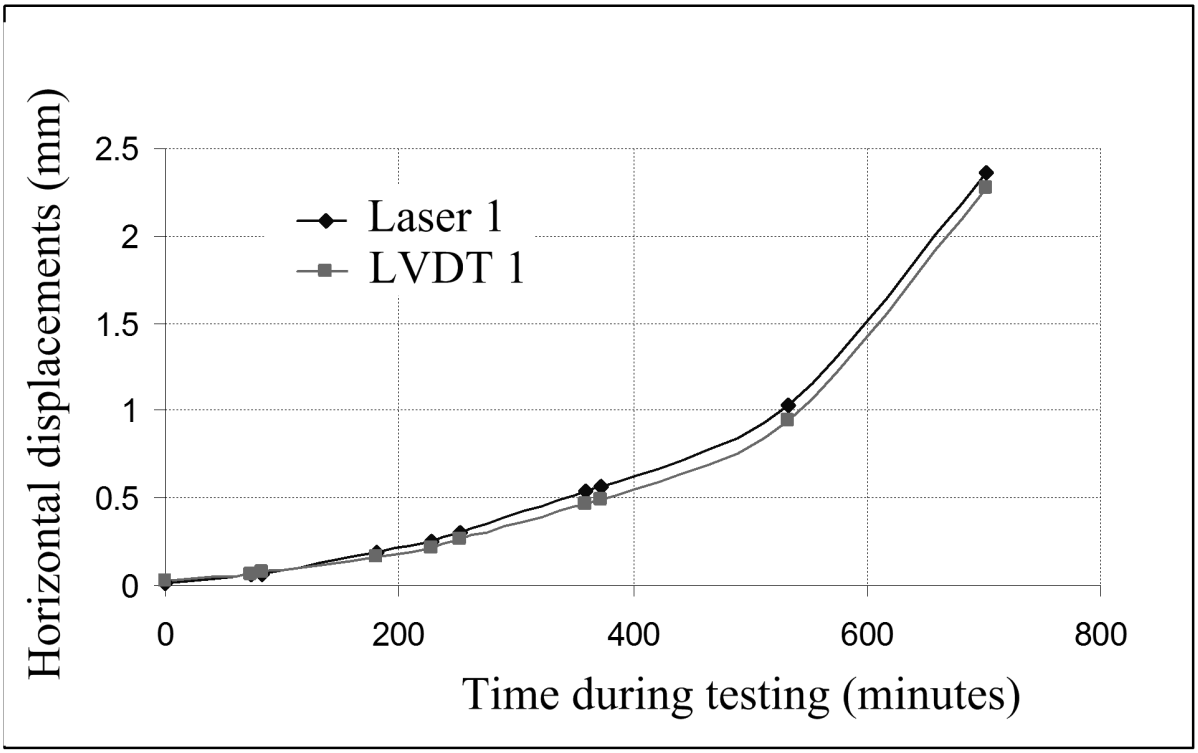

Fig. 11 – Surface soil settlement (in model scale) behind the wall - LVDT 1 and Laser 1 instruments comparison

Digital images were taken after every 6-second drainage interval (simultaneous drainage of water and heavy fluid); the 6-second drainage interval corresponded to a 1m excavation at prototype scale. An 8-megapixel digital camera, with a field of view of dimensions 185mm by 125mm resulted in a pixel size of 0.05mm by 0.05mm. The patch size used for this research was 64pixels by 64 pixels, which is equivalent to a square of side 3.2mm. Therefore, the patch covers an area that is about 665 times that of the area covered by a sand particle of size 0.14mm (D_{50} of the sand used in this study). Fig. 12 shows the comparison between the soil settlement profile obtained by the lasers and LVDTs and the soil profile obtained by the PIV at model scale at a depth equivalent to 8m-excavation level at prototype scale. The curvature of the two profiles agreed quite well but the PIV displacements were slightly less than the displacements reported by the lasers and LVDTs. This was due to friction between the sand and the laminated glass sheet.

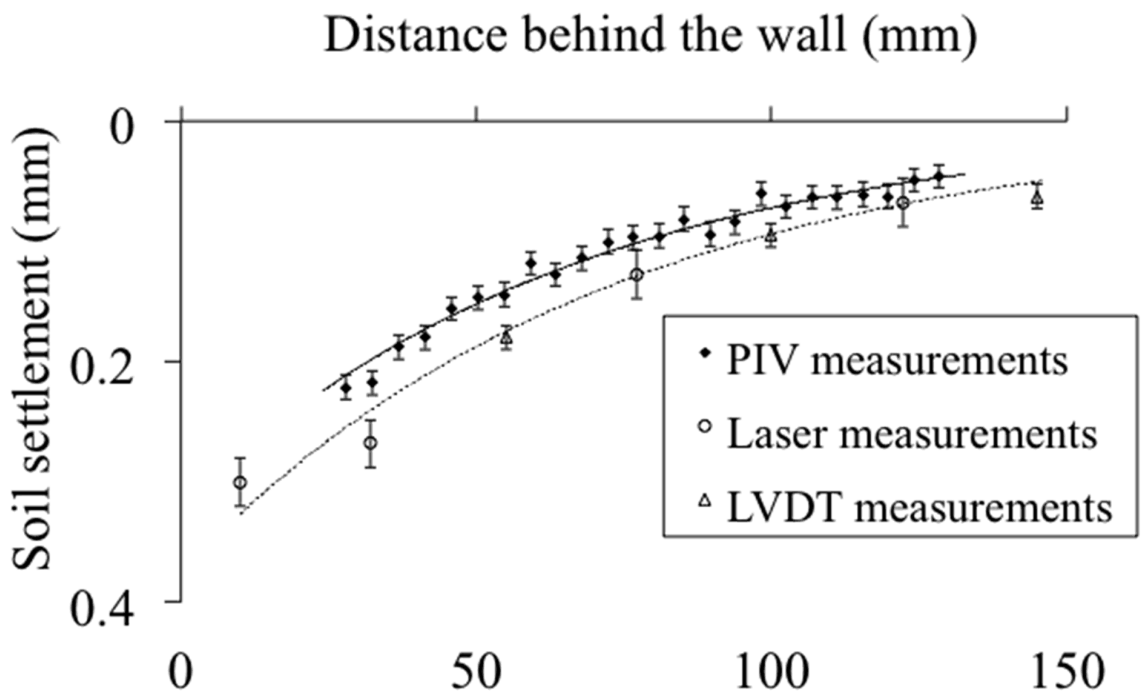

Fig. 12 – Comparison between the PIV and other instruments (LVDTs and lasers) measurements – soil surface settlement at 106.7mm drop (8m Exc.)

A comparison was then made between the results of test MEGF3 and other data published from different sources in the literature to investigate the reliability of the centrifuge data from test MEGF3. Some of the comparisons made are as follows:

- The centrifuge test results reported by King and McLoughlin (1992) for cantilever retaining walls in dry sand at 50g provide the opportunity to compare the results of test MEGF3 at 75g to results for similar centrifuge tests. Fig. 13 shows a comparison between the results of test MEGF3 and the results obtained from King and McLoughlin (1992). The maximum horizontal wall displacements, normalized by excavation depth (h), are plotted against the excavation depth (h) normalized by the embedment depth (d). The embedment depth is calculated by subtracting the excavation depth (h) from the total depth of the wall. In Fig. 13, up to a normalised excavation depth of about 1, the

data points from test MEGF3 follow the data reported by King and McLoughlin (1992) very closely. Beyond a normalised excavation depth value of about 1, the centrifuge data points and the data from King and McLoughlin (for dense sand and rough wall) start diverting significantly. At prototype scale, the wall used by King and McLoughlin (1992) was 11m in height while the wall used in test MEGF3 was about 17m in height. Therefore, with increasing (h/d) values the factor of safety against overturning for the wall used by King and McLoughlin (1992) drops more rapidly than the wall of test MEGF3. Thus more wall displacements would be expected.

- Clough and O'Rourke (1989) summarised field case studies where movements could be related solely to excavation construction. The maximum normalised wall horizontal displacement (w/h) recorded by test MEGF3 was 0.38%, which compares reasonably well with the maximum value of 0.5% reported by Clough and O'Rourke (1989).
- The maximum normalised wall horizontal displacement (w/h) of 0.38% and the maximum normalised soil settlement (S_v / h) of 0.2% recorded in test MEGF3 both agree quite well with the values reported by Long (2001) for retaining walls in stiff soils. He reported average values of 0.4% and 0.2% for normalised maximum wall horizontal displacement and normalised maximum soil settlement respectively, for cantilever walls embedded in stiff soils. Long et al. (2002) reported that the normalised wall deflections (w/h) were confined within a relatively narrow band and had an average value of about 0.36%. This also agrees very well with 0.38% measured in test MEGF3 (at a FoS of about 1.5).

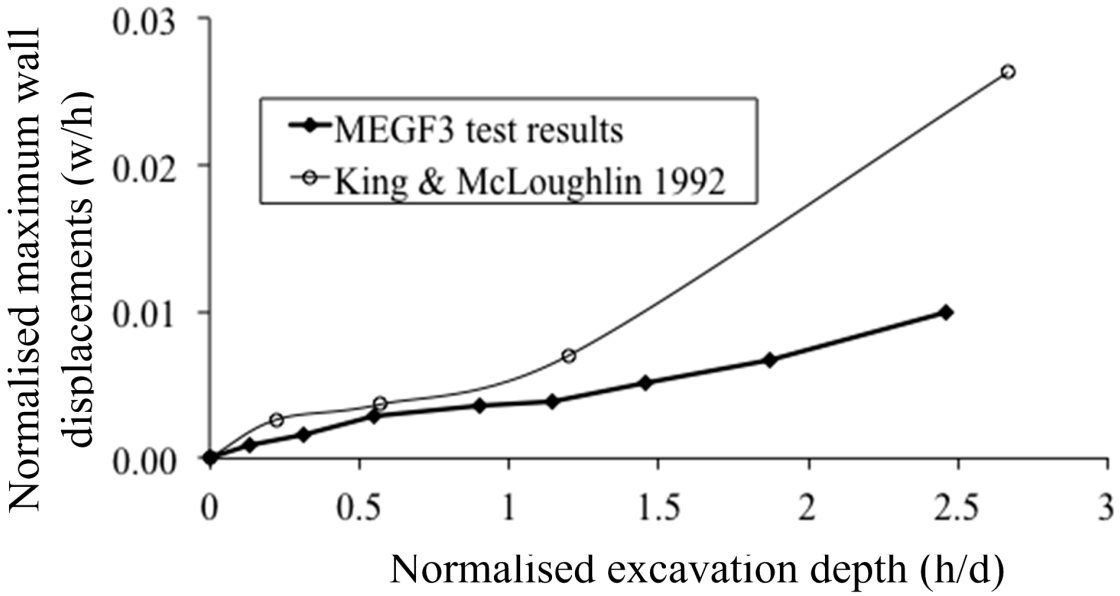

Fig. 13 – Comparison of maximum wall displacements

The good agreement of the results from test MEGF3 and other results published in the literature provided confidence that the free-field test gave reasonably realistic soil movements. This paved the way to move to the next step and introduce a stiff model building on the surface of the retained soil to investigate the soil-structure interaction during excavation simulation.

Stiff Building Test

Fig. 14 shows a schematic diagram for test MEST3, using a model building of 30mm thickness. In plan view, the model building covered the entire width of the soil sample (140mm) to maintain the plane strain condition. The objective behind the test was to study the effect of the model building's stiffness on the excavation induced displacements. The results are reported in this paper at an excavation depth of 106.7mm at model scale (8m excavation in prototype scale). The interface between the model building and the soil was rough. Figs. 15a and 15b show the settlement and horizontal displacements of block MEST3 and the soil surface beneath the block. The free-field displacements of test MEGF3 are also shown for comparison.

- The settlement data points for the soil surface and the model building are in good agreement. The data indicate that the settlement of the model is slightly larger than the soil settlement. When compared to the free-field settlement, the block and the soil surface immediately beneath did not exhibit any significant curvature. The data points indicate that the block (and the soil beneath) simply tilted as a result of the excavation. Because of its high stiffness, the model building only tilted, exhibiting no curvature. The presence of the model block modified the settlements of the soil underneath it compared to the free-field scenario.
- Horizontally, both the block and the soil surface beneath moved almost uniformly when compared to the free-field horizontal displacements. The stiffness of the block had a big influence on the soil surface horizontal displacements. Fig. 15b shows that a relative slip had occurred between the block and the soil, with the soil moving more towards the excavation than the block. The horizontal strains from the free-field scenario has not been transmitted to the model building because of the slippage at the soil/model building interface.

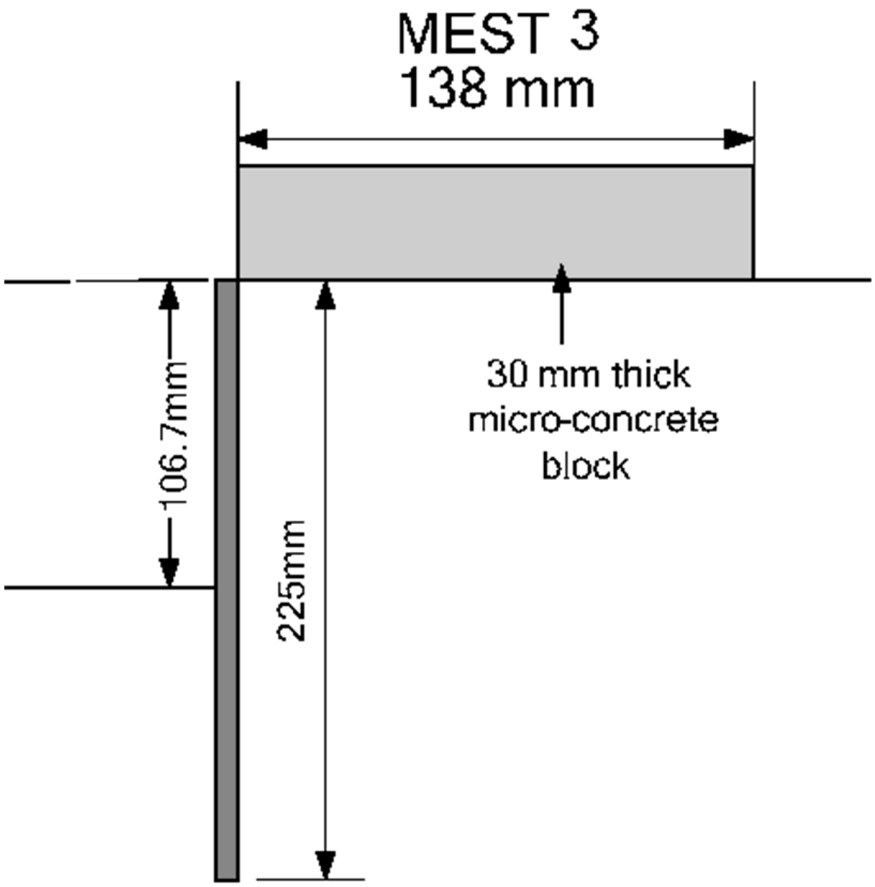

Fig. 14 – Schematic diagram for test MEST3 (stiff building test)

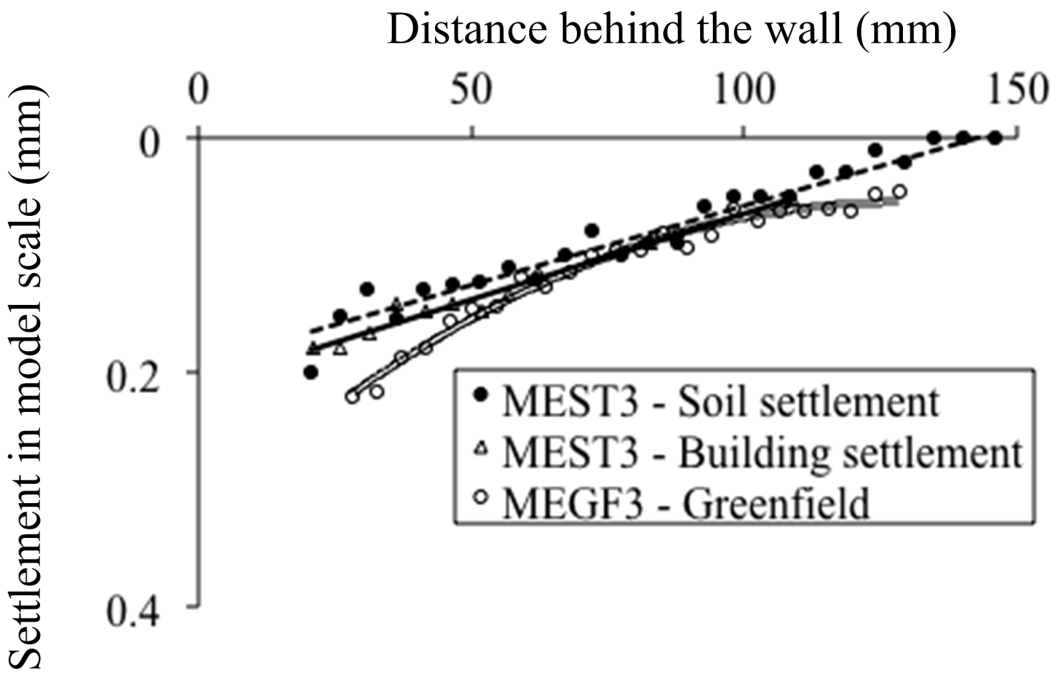

Fig. 15a – Soil-building-greenfield settlement comparison

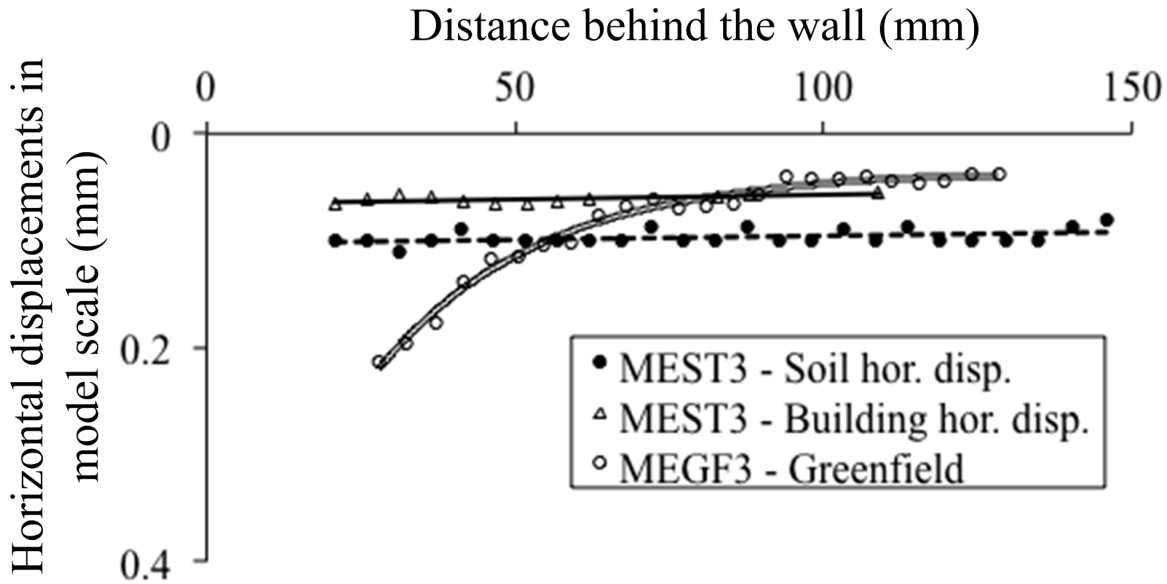

Fig. 15b – Soil-building-greenfield horizontal displacement comparison

Conclusions

Centrifuge model tests of excavations in sand were carried out using a newly developed two-fluid technique, which simulates the simultaneous removal of vertical and horizontal stresses in a more realistic manner. Before excavation starts, the new method provides initial ground conditions that result in some movement for the retaining wall and the retained soil. The performance of a typical model excavation procedure was monitored using a variety of instruments designed with an appropriate degree of redundancy to detect any errors. Simultaneous removal of vertical and horizontal stresses (simulating excavation), and measurements of ground deformations and retaining wall movements were successfully demonstrated. In one of the tests reported in this paper (test MEST3) a thick micro-concrete block, representing a stiff building, was placed behind the retaining wall to investigate its effect when compared to the free-field scenario (test MEGF3). Settlement results confirm that a stiff building behind the retaining wall only tilts during excavation with very little curvature exhibited. The soil underneath, constrained by the building above, has no option but to follow the settlement profile of the building. Horizontally, the stiff building moved uniformly towards the excavation with no horizontal strain developing. The soil underneath, again constrained by the building above, had to move horizontally, almost uniformly, but with a smaller magnitude and slip occurring between the soil and the building.

The digital image analysis using the PIV technique enabled the development of the complete soil deformation mechanism to be displayed as an incremental process during each stage of excavation. The accuracy of PIV in determining the development of lateral wall movements and ground settlements was cross-checked by the use of LVDTs and laser displacement transducers, and plane strain test conditions were confirmed. The observed deformation mechanisms confirm that stiff buildings affected by excavation-induced displacements tilt and sustain very little or no curvature. They also experience very little, if any, horizontal strains. This has been

seen in many field case studies reported in the literature. The practical importance of taking the buildings' stiffness into account, in the three-stage building damage assessment process (Mair, 2003) is therefore emphasized.

The centrifuge tests presented in this paper studied the effect of a stiff model building on excavation-induced displacements. The test results have shown that soil-structure interaction problems could be studied in great detail using the centrifuge. In future, the model building could adopt different foundations including spread footings and piles. In addition, model buildings can be positioned to have a skew angle with respect to the retaining wall (in plan view). This would enable the investigation of twist deformations in the centrifuge.

Acknowledgements

The authors would like to thank all staff at the Schofield Center for their help with the experimental set-up. The authors would also like to acknowledge the financial support provided by the Cambridge Commonwealth Trust and the Gates Cambridge Trust.

REFERNCES

Arthur, J.R.F., 1962, "Strains and lateral force in sand," PhD thesis, University of Cambridge.

Bolton, M.D. and Powrie, W., 1987, "Collapse of diaphragm walls retaining clay," Geotechnique, volume 37, No. 3, pp 335 – 353.

Bransby, P.L, and Milligan, W.E., 1975, "Soil deformations near cantilever sheet pile walls," Geotechnique, volume 25, No.2, pp 175-195.

Burland, J.B., 1995, "Assessment of risk of damage to buildings due to tunnelling and excavations," Invited special lecture, in the Proceedings of the 1st International Conference on Earthquake and Geotechnical Engineering, ISTokyo' 95, 1189-1201.

Burland, J.B. and Wroth, C.P., 1974, "Settlement of buildings and associated damage. State of the Art review." Conference on settlement of structures, Cambridge, Pentch Press, London, 611 – 654.

Burland, J,B., Broms, B.B. and de Mello, V. F. B., 1977, "Behaviour of foundations and structures – State of the Art Report." Proceedings of the 9th International Conference on Soil Mechanics and Foundation Engineering, Tokyo, Vol.2; 495-546.

Clayton, C. R. I., and Milititsky, J., 1986, "Earth pressure and earth retaining structures", Surrey University Press, London.

Clough, G.W. and O'Rourke, T.D., 1990, "Construction induced movements of in-situ walls", ASCE Geotechnical special publication No.25 – Design and Performance of Earth Retaining structures, 439 – 470.

Elshafie, M. Z. E. B., 2008, "Effect of building stiffness on excavation-induced displacements," PhD thesis, University of Cambridge.

Franzius, J. N., 2003, "Behaviour of buildings due to tunnel induced subsidence," PhD thesis, Imperial College of Sceince, Technology and Medicine, University of London.

Franzius, J. N., Potts, D. M. and Burland, J. B., 2006, "The response of surface structures to tunnel construction," Proceedings of the Institution of Civil Engineers, Geotechnical Engineering, 159, pp. 3 – 17.

King, G.J. and McLoughlin, J.P., 1992, "Centrifuge model studies of a cantilever retaining wall in sand", Proceedings of an international conference on Retaining structures, Cambridge, 711-720.

Long, M.M., 2001, "Database for retaining wall and ground movements due to deep excavations", J. Geotech. And Geoenvironm. Eng., ASCE 127 (3): 203-224.

Madabhushi, S.P.G, Houghton, N.E. and Haigh, S.K., 2006, "A new automatic sand pourer for model preparation at University of Cambridge," ICPMG'06 – © 2006 Taylor & Francis group, London, ISBN 0-415-41586-1, pp. 217-222.

Mair, R.J, Taylor, R.N. and Burland, J.B., 1996, "Prediction of ground movements and assessment of risk of building damage due to bored tunnelling," Proceedings of the International symposium on Geotechnical aspects in soft ground- London-April 1996, pp 713-718.

Mair,R.J., 2003, "Keynote address: Research on tunnelling-induced ground movements and their effects on buildings – lessons from the Jubilee line extension" Proc. Int. Conf. Response of buildings to excavation induced ground movements, London (Ed. F.M. Jardine). CIRIA special Publication 201, CIRIA, London.

Padfield, C. J. and Mair, R. J., 1984, "Design of retaining walls embedded in stiff clay," Report 104, CIRIA, London.

Potts, D.M. and Addenbrooke, T.I., 1997, "A structures influence on tunnelling-induced ground movements," Proceedings of the Institution of Civil Engineers, Geotechnical Engineering 1997, volume 125, Issue 1, pp 109-125.

Powrie, W., 1986, "The behaviour of diaphragm walls in clay," PhD thesis, University of Cambridge.

McNamara, A.N., 2001, "Influence of heave reducing piles on ground movements around excavations," PhD thesis, City University, London.

Richards, D. J., 1995, "Centrifuge and numerical modelling of twin propped retaining walls," PhD thesis, University of London (Queen Mary and Westfield College).

Roark, R. and Young, W., 1975, " Formulas for Stress and Strain" 5th edition, McGraw-Hill, ISBN 0070530319.

Standing, J.R., 2001, "Elizabeth House, Waterloo. Volume 2: Case studies. Building response to tunnelling," Case studies from construction of the Jubilee Line Extension Burland, J. B., Standing, J. R., & Jardine, F. M. (eds).

Tan, F.S.C., 1990, "Centrifuge and theoretical modelling of conical footings on sand," PhD thesis, University of Cambridge.

Terazaghi, K., 1934a, "Large Retaining Wall Tests, I-Pressure of Dry Sand," Engineering News Record, pp 136-140.

Terazaghi, K., 1934b, "Large Retaining wall tests, II-Pressure of Dry Sand," Engineering News Record, pp 259-262.

White, D.J., Take, W.A. & Bolton, M.D., 2003, "Soil deformation measurement using particle image velocimetry (PIV) and photogrammetry," Geotechnique, volume 54, No.7, pp. 619-631.

Zhao, Y., Gafar, K., Elshafie, M.Z.E.B., Deeks, A.D., Knappett, J.A. and Madabushi, S.P.G., 2006, "Calibration and use of a new automatic sand pourer," ICPMG'06 – © 2006 Taylor & Francis group, London, ISBN 0-415-41586-1, pp. 265-270.

FIGURE CAPTIONS

Fig. 1 – Front view of the centrifuge model

Fig. 2 – Schematic diagram of the centrifuge model

Fig. 3a – Rate of drop change for water and heavy fluid

Fig. 3b – Water and heavy fluid levels measured at 75g

Fig. 4 – Water and heavy fluid drainage control setup

Fig. 5a – Schematic plan view of the model wall and strong box arrangement

Fig. 5b – Picture of the model wall located inside the strong box during preparation

Fig. 6a – Schematic view of the instrumentation in a typical centrifuge model

Fig. 6b – Picture of a centrifuge model loaded into the beam – some instrumentation indicated

Fig. 6c – Arrangement of the LVDTs and lasers in relation to the retaining wall

Fig. 7 – PIV arrangement used in the models

Fig. 8a – Retaining wall horizontal movements with increasing gravitational force

Fig. 8b – Soil settlement behind the wall with increasing gravitational force (as measured by the lasers)

Fig. 8c – Soil horizontal displacement behind the wall at 75g (measured using PIV)

Fig. 9a – Strains required for mobilisation of active and passive earth pressures (after Clayton and Milititsky, 1986)

Fig. 9b – Stress paths comparison for soil elements A and B with different initial stress conditions

Fig. 10a – Surface soil settlement (in model scale) behind the wall with increasing depth of excavation – laser and LVDT measurements

Fig. 10b – Surface soil settlement (in model scale) behind the wall as measured by PIV

Fig. 10c – Surface soil horizontal displacement (in model scale) behind the wall as measured by PIV

Fig. 10d – Normalised maximum horizontal wall displacements with increasing depth of

excavation

Fig. 11 – Surface soil settlement (in model scale) behind the wall - LVDT 1 and Laser 1 instruments comparison

Fig. 12 – Comparison between the PIV and other instruments (LVDTs and lasers) measurements – soil surface settlement at 106.7mm drop (8m Exc.)

Fig. 13 – Comparison of maximum wall displacements

Fig. 14 – Schematic diagram for test MEST3 (stiff building test)

Fig. 15a – Soil-building-Free-field settlement comparison

Fig. 15b – Soil-building-Free-field horizontal displacement comparison